Stanford Exploration Project, Report 75, November 17, 1997, pages 309–336

Wavefront propagation by local ray-tracing

Lin Zhang[1]

keywords: *velocity, ray tracing, traveltime, attributes, modeling*

ABSTRACT

I develop a new wavefront-propagation method for calculating the traveltimes and geometrical amplitudes of seismic waves in a two-dimensional velocity model. The method assumes that the given velocity field is specified on a grid formed by regular triangular cells and that the velocity within each triangular cell varies linearly. These assumptions lead to a continuous representation of the velocity field. Five attributes are assigned to the wavefront at each grid point. They are traveltime, traveltime gradient, take-off angle, curvature radius of wavefront and geometric spreading factor. The attributes of a wavefront at one corner of a triangular cell are calculated from the attributes of wavefronts at other two corners by propagating the local circular wavefront through the triangular cell under the guidance of local rays. Starting from a given source position, these local computations proceed on an expanding half hexagonal ring. The new method computes the traveltimes of multiple arrivals by disassembling a multi-valued traveltime field into several single-valued fields, and then computing each of them separately. The method is evaluated with several synthetic velocity models, and its accuracy is checked with both analytical solutions and wave equation modeling.

INTRODUCTION

The traveltimes of seismic waves can be calculated on a regular grid through the process of propagating wavefronts. Such an approach was first introduced by Vidale (1988). In Vidale's method, local planar or circular wavefronts are propagated by using a finite-difference method. Since then, many different finite-difference schemes have been developed to improve the accuracy and efficiency of traveltime calculation (Van Trier and Symes, 1991; Podvin and Lecomte, 1991; Zhang, 1991). These schemes can also be extended to calculate the geometrical amplitudes of seismic waves (Vidale and Houston, 1990; Zhang, 1991).

While these finite-difference methods are enjoying popularity in more and more

[1]**email:** not available

areas of seismic data processing, their limitations are also being revealed. Although these methods give accurate traveltimes, they may produce large errors in calculating traveltime gradients when velocity varies rapidly. Because the geometrical amplitudes honor the zeroth order transport equation that involves traveltime gradients, these errors are reflected in the amplitude calculation. The large errors in traveltime gradients are caused by the discontinuous representation of a velocity field that a finite-difference method assumes, as well as by the first-order finite-difference approximations that the method makes.

The traveltime field in a varying velocity medium is generally a multi-valued function of subsurface positions. But all existing finite-difference methods compute only the traveltime of the first arrival at each subsurface point. One reason is that the wavefront of a first arrival is always continuous; hence finite-difference approximations to the eikonal equation are valid. Another reason is that among different arrivals at a subsurface point, the first arrival is easy to identify because it has the minimum traveltime. When imaging reflection seismic data, the events corresponding to energetic arrivals should be used. However, for a complex velocity model, the energy carried by first arrivals may become considerably weaker than that carried by other later arrivals. In such a situation, the traveltimes of more energetic, later arrivals need to be computed.

This paper introduces the local ray-tracing method for wavefront propagation. Because the method assumes a continuous velocity representation and propagates local circular wavefronts by following local rays, it gives more accurate traveltimes and amplitudes than a finite-difference method. The method computes the traveltimes of multiple arrivals by disassembling a multi-valued traveltime field into several single-valued fields, and then computing each of them separately. These single-valued fields may include discontinuities that a finite difference method cannot handle. The local ray-tracing method can propagate wavefronts of discontinuities.

This paper begins with the description of a continuous representation of a velocity field. It then presents the details of the local ray-tracing method, including a local wavefront propagation scheme, a global updating scheme, and initialization. Several issues on multiple arrivals are also addressed. Finally, the accuracy of the method is examined, and several synthetic examples are used to demonstrate the method.

CONTINUOUS REPRESENTATION OF A VELOCITY FIELD

The representation of a velocity field is crucial to the accuracy and efficiency of traveltime and amplitude calculations. Because the traveltime and amplitude calculations are more accurate in a continuous velocity model than in a discontinuous velocity model, I map a given velocity field onto a grid formed by regular triangular cells. Within each triangular cell, velocity varies linearly, as follows:

$$v(x,z) = v_o + v_x(x - x_o) + v_z(z - z_o), \tag{1}$$

where two components of the velocity gradient are determined by

$$\begin{cases} v_x = \dfrac{(z_b - z_o)(v_a - v_o) - (z_a - z_o)(v_b - v_o)}{(z_b - z_o)(x_a - x_o) - (x_b - x_o)(z_a - z_o)} \\[2ex] v_z = \dfrac{(x_a - x_o)(v_b - v_o) - (x_b - x_o)(v_a - v_o)}{(z_b - z_o)(x_a - x_o) - (x_b - x_o)(z_a - z_o)}, \end{cases} \tag{2}$$

v_o, v_a and v_b are the velocities at the three corners, (x_o, z_o), (x_a, z_a) and (x_b, z_b), of the triangular cell, respectively. Figure 1 shows examples of a triangular grid and a triangular cell. With this representation, velocity is continuous everywhere, including the boundaries of adjacent triangular cells. Velocity contrasts at the interfaces of the original velocity model are approximated by triangular cells of large velocity gradients.

The reason for using linearly varying velocities within triangular cells is that seismic waves propagate along circular ray paths in a linearly varying velocity medium. Therefore, local ray-tracing in these triangular cells can be done analytically. An alternative is to use linearly varying sloth (slowness squared) within each triangular cell. The ray paths in such a medium are hyperbolas.

In a manner similar to the finite difference method developed by Vidale (1988), two schemes need to be built for the local ray-tracing method. In the following sections, I first develop the scheme used to propagate a local wavefront through a triangular cell. I then describe the scheme that addresses the order in which the local computations proceed.

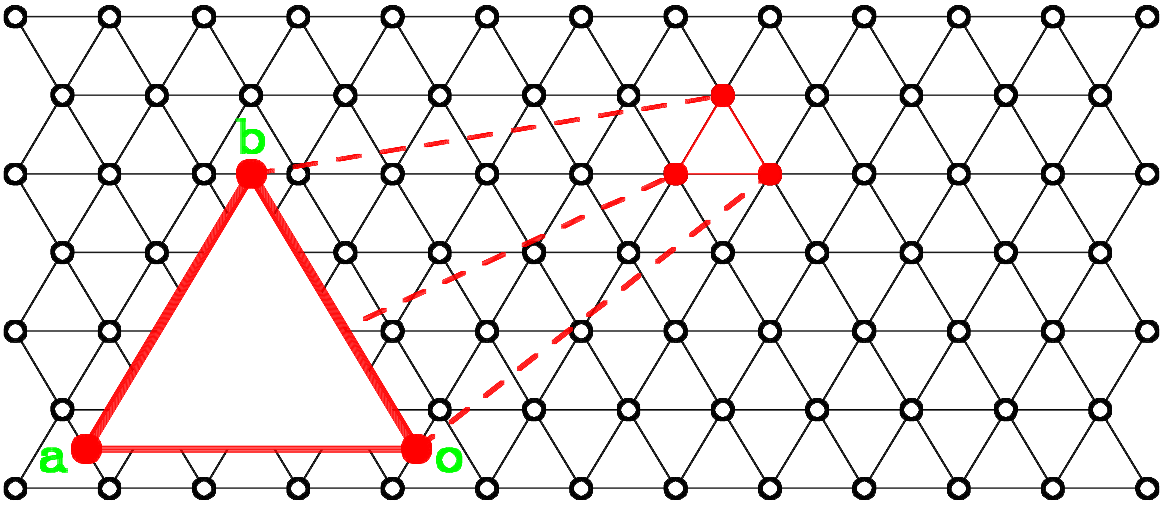

Figure 1: Examples of a triangular grid and a triangular cell. The velocity field is specified on the grid points indicated by little circles. Velocities at the three corners of a cell determines the constant velocity gradient within the cell. $\boxed{\text{lin1-vptrigrid}}$ [NR]

LOCAL WAVEFRONT PROPAGATION SCHEME

Local wavefront propagation is a process of propagating a wavefront to a grid point from its neighbors. Through this process, the attributes of a wavefront at a grid point is determined from the attributes of wavefronts at neighboring grid points.

The attributes of a wavefront

Multiple arrivals may reach a subsurface point. Whereas some arrivals are identifiable by the kinematics of seismic waves, other arrivals have to be identified by the dynamics of seismic waves. Therefore, the attributes of a wavefront should include both the kinematic parameters and the dynamic parameters of seismic waves.

The local ray-tracing method uses five wavefront attributes in the process of wavefront propagation. They are

$$\eta = \{\tau,\ (u,w),\ \gamma,\ R,\ J\}, \tag{3}$$

where τ is the traveltime for a wave to propagate from a surface point to a subsurface point, $(u,w) = (\tau_x, \tau_z)$ is the traveltime-gradient vector that points to the direction of the wave propagation at the subsurface point, γ is the take-off angle of the ray connecting the surface point and the subsurface point, R is the curvature radius of the wavefront at the subsurface point, and finally, J is the geometrical spreading factor (see its definition in Červený, 1981b) at the subsurface point. Among these attributes, τ, (u,w) and γ are related to the kinematics of wave propagation, whereas R and J are related to the dynamics.

Local ray-tracing

The local ray-tracing method propagates a wavefront locally through triangular cells of linearly varying velocities by following local rays. Because the whole process of wavefront propagation involves tracing many local rays, it is necessary to have an efficient ray-tracing algorithm. Fortunately, the analytical solutions to the ray equations for a linearly varying velocity field are well known, and the analytical solutions of R and J for such a velocity field are also known. Here I merely quote the results. The details of the derivations can be found in Telford et. al. (1976) and Červený (1981abc).

Suppose we know the attributes of a wavefront, $\eta_0 = \{\tau_0, (u_0, w_0), \gamma_0, R_0, J_0\}$, at an initial point (x_0, z_0). By tracing a ray, we can find the attributes of the wavefront, $\eta = \{\tau, (u,w), \gamma, R, J\}$, at an arbitrary point (x,z) on the ray. In a linearly varying velocity field, the two components of the velocity gradient are constant, (v_x, v_z). It is known that in such a velocity field the ray follows a circular trajectory. The traveltime is determined by integrating the inverse of velocity along the ray, which yields

$$\tau = \tau_0 + \frac{1}{g}\log\left(\frac{\sin i(1+\cos i_0)}{\sin i_0(1+\cos i)}\right), \tag{4}$$

where $g = \sqrt{v_x^2 + v_z^2}$ is the magnitude of the velocity gradient, and i_0 and i are the ray angles shown in Figure 2. It can be shown that

$$\left\{\begin{array}{lcl} \cos i_0 & = & \dfrac{v_0}{g}(v_z u_0 - v_x w_0) \\ \\ \sin i_0 & = & \dfrac{v_0}{g}(v_z w_0 + v_x u_0), \end{array}\right. \tag{5}$$

where v_0 is the velocity at the initial point. The ray angle, i, at point (x,z) is related to the arc-length of the ray path as follows:

$$i = i_0 + (s - s_0)\frac{g\cos i_0}{v_0}. \tag{6}$$

where $s - s_0$ is the arc length of the ray between two points. The two components of the traveltime gradient at the point (x,z) are determined by

$$\left\{\begin{array}{lcl} u & = & \dfrac{1}{vg}(v_z\cos i + v_x\sin i) \\ \\ w & = & \dfrac{1}{vg}(v_z\sin i + v_x\cos i) \end{array}\right. \tag{7}$$

where v is the velocity at point (x,z). Because the take-off angle of the ray does not change along the ray,

$$\gamma = \gamma_0. \tag{8}$$

Červený (1981a) shows that in a velocity field of zero second order spatial derivatives, the curvature radius of a wavefront at a point on a ray is linearly proportional to the integration of the velocity field along the ray. Because a linearly varying velocity field has zero second-order spatial derivatives, the integration of the velocity along the circular ray path gives

$$R = \frac{v_0}{v}\left[R_0 + \frac{v_0}{g\cos i_0}(1 - \frac{\cos i}{\cos i_0}).\right] \tag{9}$$

Similarly, we can show that

$$J = J_0\frac{vR}{v_0 R_0}. \tag{10}$$

where R is defined in equation (9).

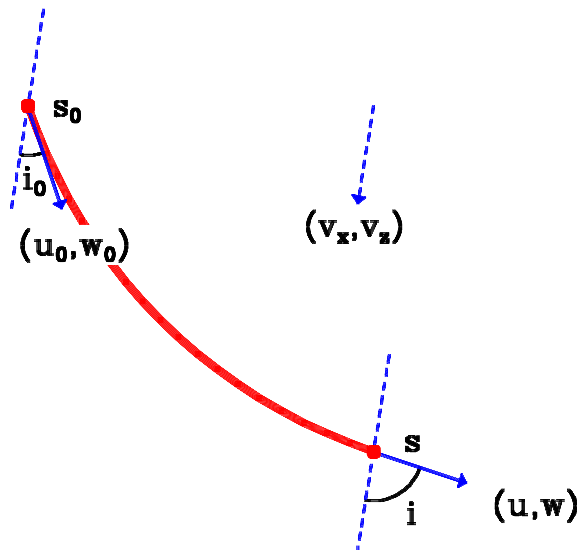

Figure 2: Ray-tracing in a linearly varying velocity field. The dash arrow shows the direction of the velocity gradient. The solid arrows show the directions of traveltime gradients that are tangential to the ray. Ray angles are measured between the direction of the velocity gradient and the directions of the ray. lin1-vpraytrc [NR]

When a ray reaches the boundary of two adjacent triangular cells, the phase matching method can be used to trace the ray across the boundary (Červený, 1981c). Traveltime τ and take-off angle γ are always continuous across the boundary. Because of the continuous velocity representation, there is no discontinuity of velocity across the boundary. Therefore traveltime gradient (u, w) and geometrical spreading factor J are also continuous at the boundary. However, curvature radius R is generally not continuous at the boundary because of the change of the velocity gradient across the boundary. Červený (1981c) derives a general formula that relates the curvature radii of wavefronts on the two sides of the boundary. This general formula can be greatly simplified by considering that the velocity field is continuous at the boundary and that the boundary has a zero curvature. The result is

$$R^+ = \frac{R^-}{1 + vIR^-} \tag{11}$$

where R^+ and R^- are the curvature radii before and after crossing the boundary, respectively, I is a factor defined as follows:

$$\begin{aligned} I \;\; = \;\; & \frac{2\tan\theta}{v^2}\left[\cos\phi(v_x^+ - v_x^-) - \sin\phi(v_z^+ - v_z^-)\right] + \\ & \frac{\tan^2\theta}{v^2}\left[\sin\phi(v_x^+ - v_x^-) + \cos\phi(v_z^+ - v_z^-)\right]. \end{aligned}$$

As shown in Figure 3, θ is the incident angle of the ray to the normal of the boundary, ϕ is the angle between the orientation of the boundary and the z-axis, and (v_x^-, v_z^-) and (v_x^+, v_z^+) are the velocity gradients of two adjacent cells, respectively.

Finite difference methods propagate local wavefronts in cells of constant velocity. Because wavefronts propagate along straight rays in a constant velocity field, local

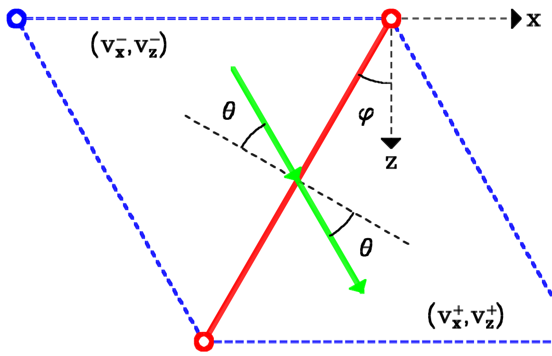

Figure 3: Ray-tracing across a boundary of two triangular cells. Because the velocity is continuous at the boundary, the angle of incidence is equal to the angle of refraction. lin1-vpbound [NR]

ray-tracing is trivial. The local-plane-wave assumption implies that $R \to \infty$. All these simplifications make finite difference methods more efficient than the local ray-tracing method. Of course, they also reduce the accuracy of the computations.

Propagating local circular wavefronts

A wavefront can be locally propagated by tracing local rays. Figure 4 shows a cell in a triangular grid. At two corners of the triangular cell, the attributes of the wavefront are known to be

$$\eta_a = \{t_a, (u_a, w_a), R_a, \gamma_a, J_a\}$$

and

$$\eta_b = \{t_b, (u_b, w_b), R_b, \gamma_b, J_b\},$$

respectively. The wavefront attributes at the third corner,

$$\eta_o = \{t_o, (u_o, w_o), R_o, \gamma_o, J_o\}$$

can be determined through a procedure of propagating a local wavefront that passes the line boundary between the points a and b.

The procedure begins with local ray-tracing from two corners of the triangular cell, where the attributes of wavefronts are known. As shown in Figure 4, the ray a shoots from the point a and in the direction of the gradient vector (u_a, w_a), and the ray b shoots from the point b and in the direction of the gradient vector (u_b, w_b). These two rays form a ray-tube that guides the propagation of the local wavefront passing between the points a and b. If a point on the local wavefront follows the wavefront propagation and reaches the third corner of the triangle, it must cross the boundary ab and propagate through the triangular cell. Therefore, the two local rays are traced as if the straight-line boundary ab extends out at both ends and the velocity field within the triangular cell extends out with the velocity gradient being

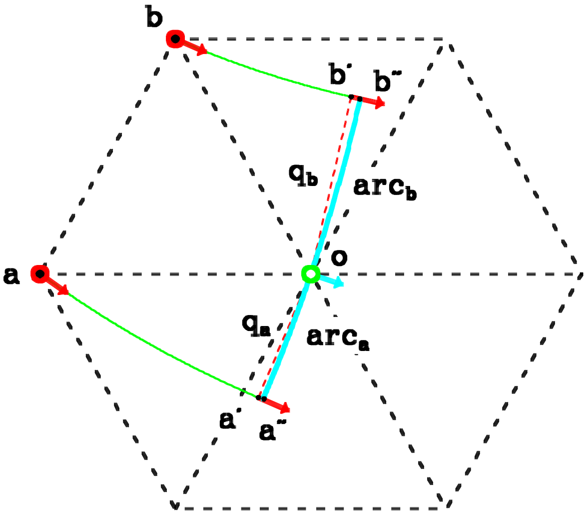

Figure 4: Local wavefront propagation when the wavefront attributes at the points a and b are associated with a common wavefront. By tracing two local rays, the wavefront attributes at the point o is determined from the wavefront attributes at the points a and b jointly. lin1-vpwftprg1 [NR]

unchanged. The wavefront attributes at any point on the rays can be calculated by using the formulas presented in the last section.

As shown in Figure 4, the local rays a and b are traced to the points a' and b', respectively. At these two points, the normal distances from the third corner of the triangular cell to the rays are achieved. Let q_a and q_b denote the two normal distances, and define

$$\begin{aligned} q_a &= v_{a'}w_{a'}(x_{a'} - x_o) - v_{a'}u_{a'}(z_{a'} - z_o) \\ q_b &= v_{b'}w_{b'}(x_{b'} - x_o) - v_{b'}u_{b'}(z_{b'} - z_o), \end{aligned}$$

where (x_o, z_o) are the coordinates of the third corner of the triangular cell, $(v_{a'}u_{a'}, v_{a'}w_{a'})$ and $(v_{b'}u_{b'}, v_{b'}w_{b'})$ are the unit vectors tangential to the rays at the normal points $(x_{a'}, z_{a'})$ and $(x_{b'}, z_{b'})$, respectively. With this definition, the normal distance is positive when a ray is on one side of the point o, and negative when a ray is on the other side. To ensure that the attributes of the wavefront at the point (x_0, z_0) is computed by propagating the local wavefront passing the line boundary between the points a and b, it is required that the point (x_o, z_o) is within the ray tube formed by the rays a and b. This condition is satisfied when $q_a \leq 0$ and $q_b \geq 0$.

Because the normal points a' and b' are on the rays, the attributes of the wavefront at these points can be computed analytically. Let $R_{a'}$ be the curvature radius of the wavefront at the normal point a'. Then, the curvature center of the wavefront at the point is

$$\left\{ \begin{aligned} x_{a0} &= x_{a'} - v_{a'}u_{a'}R_{a'} \\ z_{a0} &= z_{a'} - v_{a'}w_{a'}R_{a'}. \end{aligned} \right. \tag{12}$$

Similarly, the curvature center of the wavefront at the normal point b' is

$$\begin{cases} x_{b0} = x_{b'} - v_{b'} u_{b'} R_{b'} \\ z_{b0} = z_{b'} - v_{b'} w_{b'} R_{b'}, \end{cases} \tag{13}$$

where $R_{b'}$ is the curvature radius of the wavefront at the point.

The local wavefront within the ray tube formed by the rays a and b is considered to be continuous if one of the following two sets of conditions are satisfied:

1. $R_{a'} > 0$, $R_{b'} > 0$ and $w_{a'} u_{b'} - u_{a'} w_{b'} > 0$.
2. $R_{a'} < 0$, $R_{b'} < 0$ and $w_{a'} u_{b'} - u_{a'} w_{b'} < 0$.

The first set of conditions define a divergent local wavefront and the second set a convergent local wavefront. Figure 5 displays examples of these two cases. If neither of the two sets of conditions hold, the local wavefront is considered to be discontinuous. Figure 6 displays two examples.

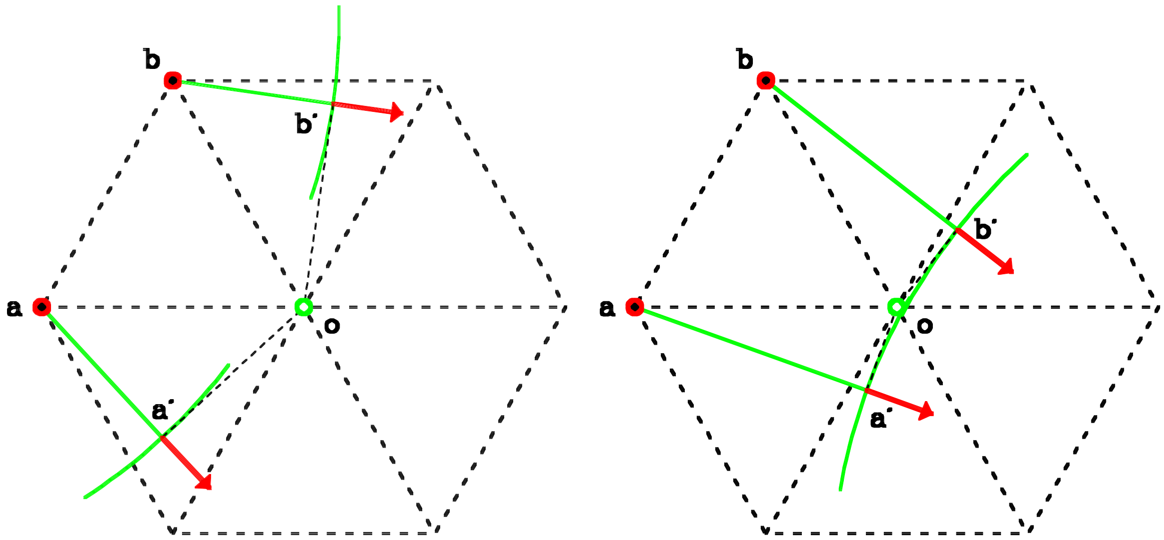

Figure 5: Continuous local wavefronts. Left: a divergent local wavefront. Right: a convergent local wavefront. lin1-vpwptype1 [NR]

When the local wavefront is continuous, the attributes at the points a and b are associated with a common wavefront. Therefore, the curvature center of the wavefront at the point o is estimated by averaging the curvature centers of the wavefront at the points a' and b' as follows:

$$\begin{cases} x_{o0} = \alpha x_{a0} + \beta x_{b0} \\ z_{o0} = \alpha z_{a0} + \beta z_{b0}, \end{cases} \tag{14}$$

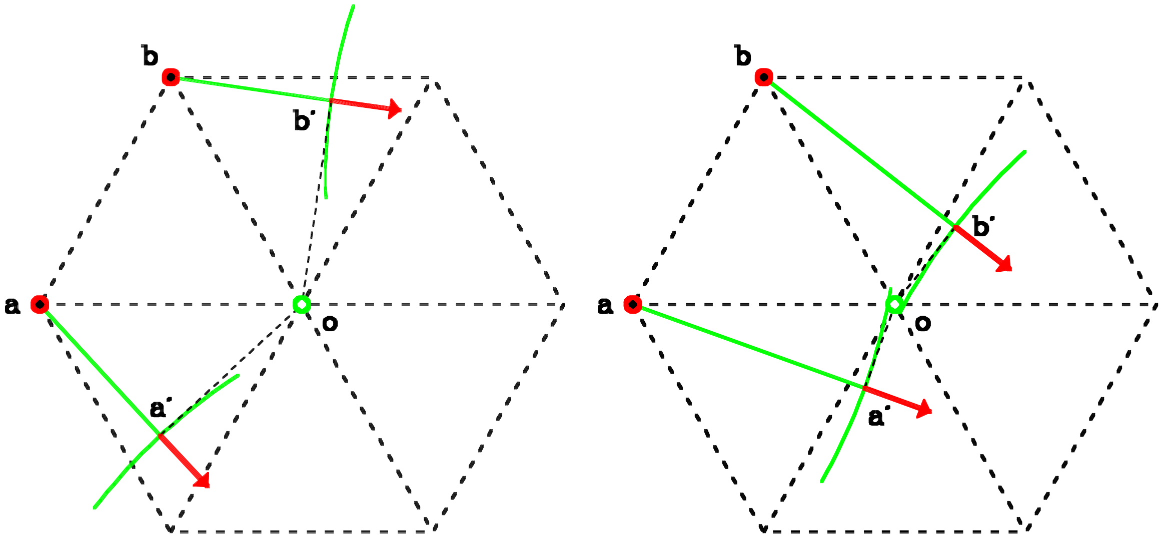

Figure 6: Two examples of discontinuous local wavefronts. lin1-vpwptype2 [NR]

where α and β are weighting coefficients determined by the normal distances, as follows:

$$\begin{cases} \alpha = \dfrac{|q_b|}{|q_b| + |q_a|} \\ \beta = \dfrac{|q_a|}{|q_b| + |q_a|} \end{cases} \tag{15}$$

The curvature radius of the wavefront at the point is then computed by

$$R_o = \mathrm{sgn}(R_{a'} + R_{b'})\sqrt{(x_o - x_{o0})^2 + (z_o - z_{o0})^2}, \tag{16}$$

and two components of the traveltime gradient by

$$\begin{cases} u_o = \dfrac{(x_o - x_{o0})}{v_o R_o} \\ w_o = \dfrac{(z_o - z_{o0})}{v_o R_o} \end{cases} \tag{17}$$

where v_o is the velocity at the point o.

The wavefront at the point o is approximated by a local circular wavefront of radius R_o and centered at (x_{o0}, z_{o0}). As shown in Figure 4, the local circular wavefront at the point o intersects with the ray a at the point a'' and the ray b at the point b''. Because these two points are on the rays, the attributes of wavefronts can be calculated analytically. Let $t_{a''}$ and $t_{b''}$ be the traveltimes at two intersections. Because both the point a'' and the point b'' are on the local circular wavefront defined at the point o, the weighted average of $t_{a''}$ and $t_{b''}$ is used to estimate the traveltime at the point o, that is

$$t_o = \alpha t_{a''} + \beta t_{b''} \tag{18}$$

where α and β are defined in equation (15). It can be shown that in a linearly varying velocity field the geometrical spreading factor function J varies along a wavefront in proportion to the velocity. Therefore, the estimate of the geometrical spreading factor J_o from the attributes at the point a'' is $v_o J_{a''}/v_{a''}$ and from point b'' is $v_o J_{b''}/v_{b''}$. The average of two gives

$$J_o = \alpha \frac{v_o}{v_{a''}} J_{a''} + \beta \frac{v_o}{v_{b''}} J_{b''} \tag{19}$$

The last parameter to be estimated is the take-off angle of the ray that reaches the point o. It can be shown that, in two-dimension,

$$J = \frac{\partial \gamma}{\partial n},$$

where n is the distance normal to the ray. Therefore, we have

$$\begin{aligned} \Delta\gamma &= \int \frac{1}{J} dn \\ &\approx \frac{1}{\bar{J}} \Delta arc, \end{aligned}$$

where $\bar{J}$ is the average geometrical spreading factor over the arc length Δarc. If the average of J_o and $J_{a''}$ is used to approximate the $\bar{J}$ over arc_a and the average of J_o and $J_{b''}$ over arc_b, then γ_o is estimated by the weighted averaging as follows:

$$\gamma_o = \alpha(\gamma_{a''} - \frac{2arc_a}{J_o + J_{a''}}) + \beta(\gamma_{b''} - \frac{2arc_b}{J_o + J_{b''}}). \tag{20}$$

With equations (16) to (20), we can compute the attributes of the wavefront at the third corner of the triangular cell.

When the local wavefront is discontinuous, the attributes at the points a and b are associated with different wavefronts. Therefore the local wavefront at each point should be propagated individually. Figure 7 shows an example in which the local wavefront at the point b is propagated. In this case, the curvature center of the wavefront at the point o is assumed to coincide with the curvature center of the wavefront at the point b', that is, $x_{o0} = x_{b0}$ and $z_{o0} = z_{b0}$. The curvature radius is then

$$R_o = \text{sgn}(R_{b'})\sqrt{(x_o - x_{o0})^2 + (z_o - z_{o0})^2}. \tag{21}$$

The formula for computing the components of the traveltime gradient at the point o is identical to equation (17). The traveltime t_o, geometrical spreading factor J_o and take-off angle γ_o are computed by simply setting $\alpha = 0$ and $\beta = 1$ in equations (18), (19) and (20).

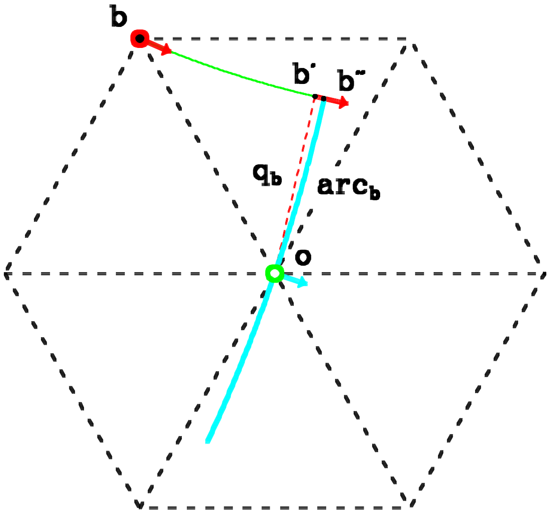

Figure 7: The local wavefront propagation when the wavefront attributes at the points a and b are associated with different wavefronts. The wavefront attributes at the point o is determined from the wavefront attributes at each point (the point b as an example) separately. lin1-vpwftprg2 [NR]

There are two special cases in which the rays a and b do not form a ray-tube because of multiple arrivals. Figure 8 shows examples of two such cases. In both cases, the rays a and b converge with each other, that is

$$w_{a'}u_{b'} - u_{a'}w_{b'} < 0.$$

The first case has $q_a < 0$ and $q_b < 0$. The ray a guides the propagation of the local wavefront passing between the points a and b, whereas the ray b guides the propagation of another local wavefront. Therefore, only the ray a is used to compute the attributes of the wavefront at the point o. The second case has $q_a > 0$ and $q_b > 0$. The ray b, instead of the ray a, is used in the computation.

The wavefront may be diffracted at the points a and b because of the changes of the velocity gradients in the adjacent triangular cells. Figure 9 shows an example of diffraction at the point b. Two rays that are traced with the same initial conditions at the point b split towards two sides. The local wavefront corresponding to diffraction is defined between two rays. The attributes of the diffracted wavefront are computed by tracing the local ray connecting the points b and o.

GLOBAL UPDATING SCHEME

With the local computations for propagating wavefronts, the attributes of wavefronts can be found throughout the grid by following a global updating scheme. The global

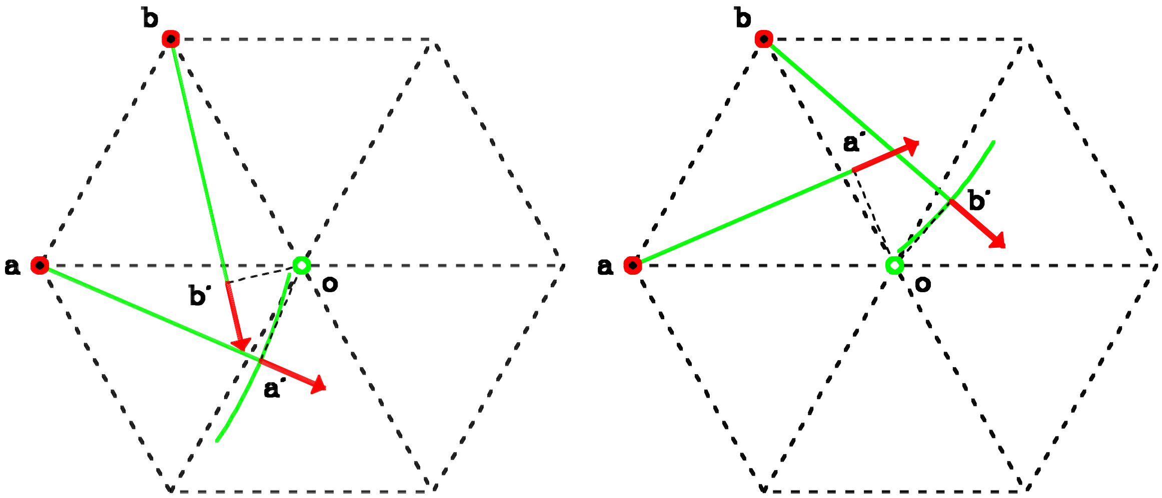

Figure 8: Two examples of local wavefronts of multiple arrivals. lin1-vpwptype3 [NR]

Figure 9: An example of a diffracted local wavefront at the point *b*. lin1-vpwftprg3 [NR]

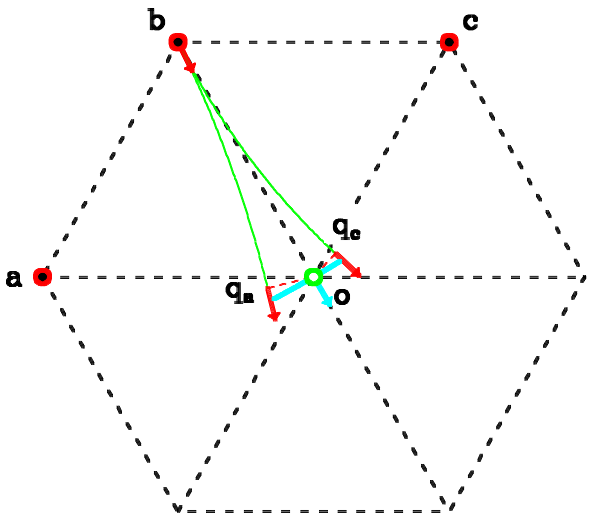

updating scheme describes the order in which local wavefront propagations proceed. This section presents a scheme that assumes a point source on the earth's surface. However, it is not difficult to generalize the scheme to an arbitrary source position.

Initialization

Since I use a triangular grid, the process of wavefront propagation proceeds on an expanding half hexagonal ring centered at the source point. To start the process, the attributes of wavefronts are initialized at the grid points inside and on a half hexagonal ring shown in Figure 10. The radius of this half hexagonal ring is determined based on the velocity field around the source point. Generally, it is chosen to be the radius of the largest half hexagon within which the velocity field is well approximated by a linear function. Such a choice make it possible to compute analytically the attributes of wavefronts at the grid points inside and on this half hexagonal ring.

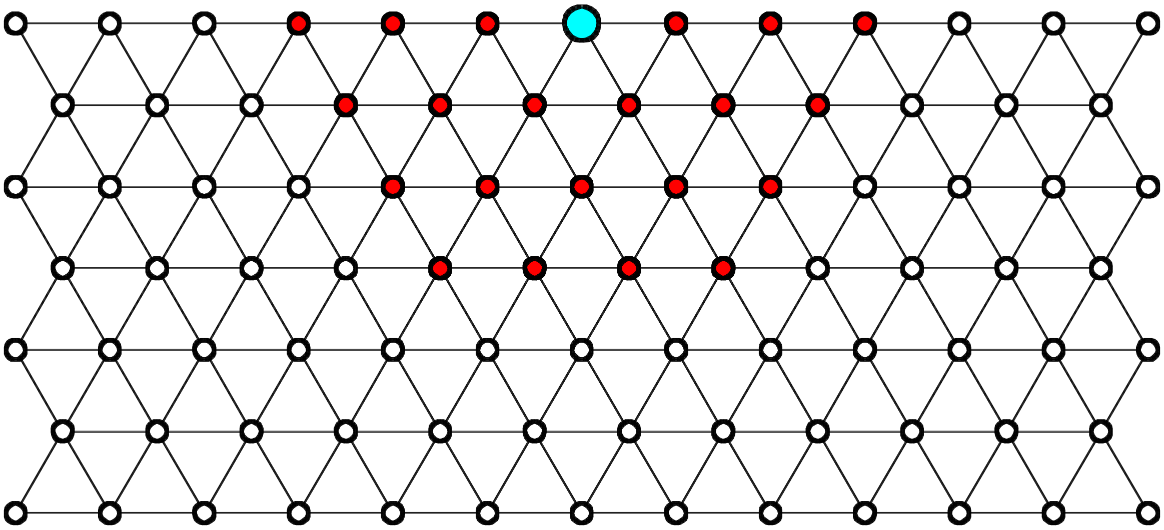

Figure 10: The attributes of wavefronts are initialized at the grid points within and on a half hexagonal ring as indicated with small black dots. The large black dot indicates the source point. $\boxed{\text{lin1-vpinit}}$ [NR]

Three phases of the updating scheme

From the initial half hexagonal ring on which the attributes of wavefronts are computed analytically, the process of wavefront propagation follows the expansion of the ring step by step. Suppose that the attributes of wavefronts are known at all the grid points within and on the half hexagonal ring of radius 4 shown in Figure 11. At the grid points on the three sides of the half-hexagon of radius 5, the attributes of wavefronts are unknown and to be computed by one step of the updating scheme. I refer to these grid points as target points. For each target point, there are six triangular cells attached to it. Each of these triangular cells has one boundary across which a local wavefront may propagate towards the target point. Figure 11 shows an example in which six boundaries associated with a target point are labeled from 1 to 6. Because seismic waves seldom propagate towards the source point, it is reasonable to assume that no local wavefront propagates into the half hexagonal ring of radius 5. With this assumption, local wavefronts that reach the target point must pass the boundaries 1, 2 or 3 shown in Figure 11. Therefore, one step of updating scheme consists of three phases. In the first phase, the local wavefront passing the boundary 1 is propagated. The second and third phases propagate the local wavefronts passing the boundaries 2 and 3, respectively. Each phase also involves the process of checking the possible diffractions at the two ends of the corresponding boundary.

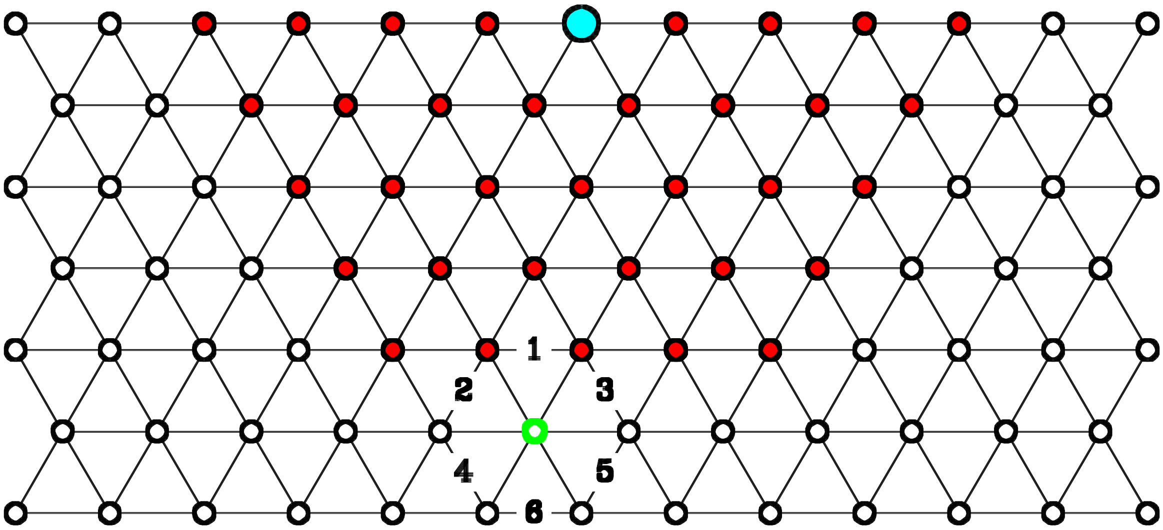

Figure 11: The attributes of wavefronts are known at the grid point inside and on the half hexagonal ring of radius 4, which are indicated by small black dots. The large black dot indicates the source point. Six boundaries associated with a target point are labeled from 1 to 6. $\boxed{\text{lin1-vpgus}}$ [NR]

Figure 12 shows how the wavefront propagation in each of the three phases proceeds globally. Because the boundary 1 associated with a target point is always on the half hexagonal ring of radius 4, the attributes of wavefronts are known at the two ends of the boundary. Therefore, in the first phase, local wavefronts are propagated towards the corresponding target points independently. The situation is different in the second phase. For each target point, one end of the boundary 2 is at another target point where the attributes of wavefronts may be unknown. Therefore, local wavefronts are propagated sequentially and count-clockwise, as shown in Figure 12. The propagation of a local wavefront is initiated at a target point when the attributes of wavefronts are known at the both ends of the boundary 2 associated with the target point. The propagation terminates when the attributes of wavefronts are unknown at one end of the boundary 2. Similarly, in the third phase, local wavefronts are propagated sequentially, but clockwise.

After the three phases of wavefront propagations, the attributes of wavefronts at all target points are computed. The half hexagonal ring increases its radius by one grid size for the computation of the next step. This process is repeated until the expanded half hexagonal ring covers all the grid points of the given model.

Multiple arrivals

When a grid point has multiple arrivals, three phases of wavefront propagations give different results of the attributes of wavefronts. The following rules are used to select a specific arrival.

- First arrival: minimum t_o.
- Most energetic arrival: minimum J_o.
- Left-going arrival: minimum u_o.
- Right-going arrival: maximum u_o.
- Up-going arrival: minimum w_o.
- Down-going arrival: maximum w_o.

Because these rules are defined locally, they don't generally ensure the global selections. The first arrival is an exception. Selecting minimum traveltimes at all steps of local wavefront propagations yields global minimum traveltimes. This result can be explained by the fact that traveltime is a monotonically increasing function along a ray. Other attributes of wavefronts do not have this property. For example, the geometrical spreading factor J may increase or decrease along a ray. Thus, the method may give locally most energetic arrivals, instead of globally most energetic arrivals.

NUMERICAL RESULTS

Using synthetic velocity models, I first examine the accuracy of the local ray-tracing method by comparing its results with the analytical solutions and the results of wave-equation modeling. I then show the results of the traveltime calculations for multiple arrivals.

Accuracy

I examine the accuracy of the local ray-tracing method with three synthetic velocity models. The first one is a constant gradient velocity model shown in Figure 13. The velocity is 1. km/s at the upper-left corner of the model. The magnitude of the velocity gradient is 6.56 1/s, and the direction is 70 degrees to the right of the depth axis.

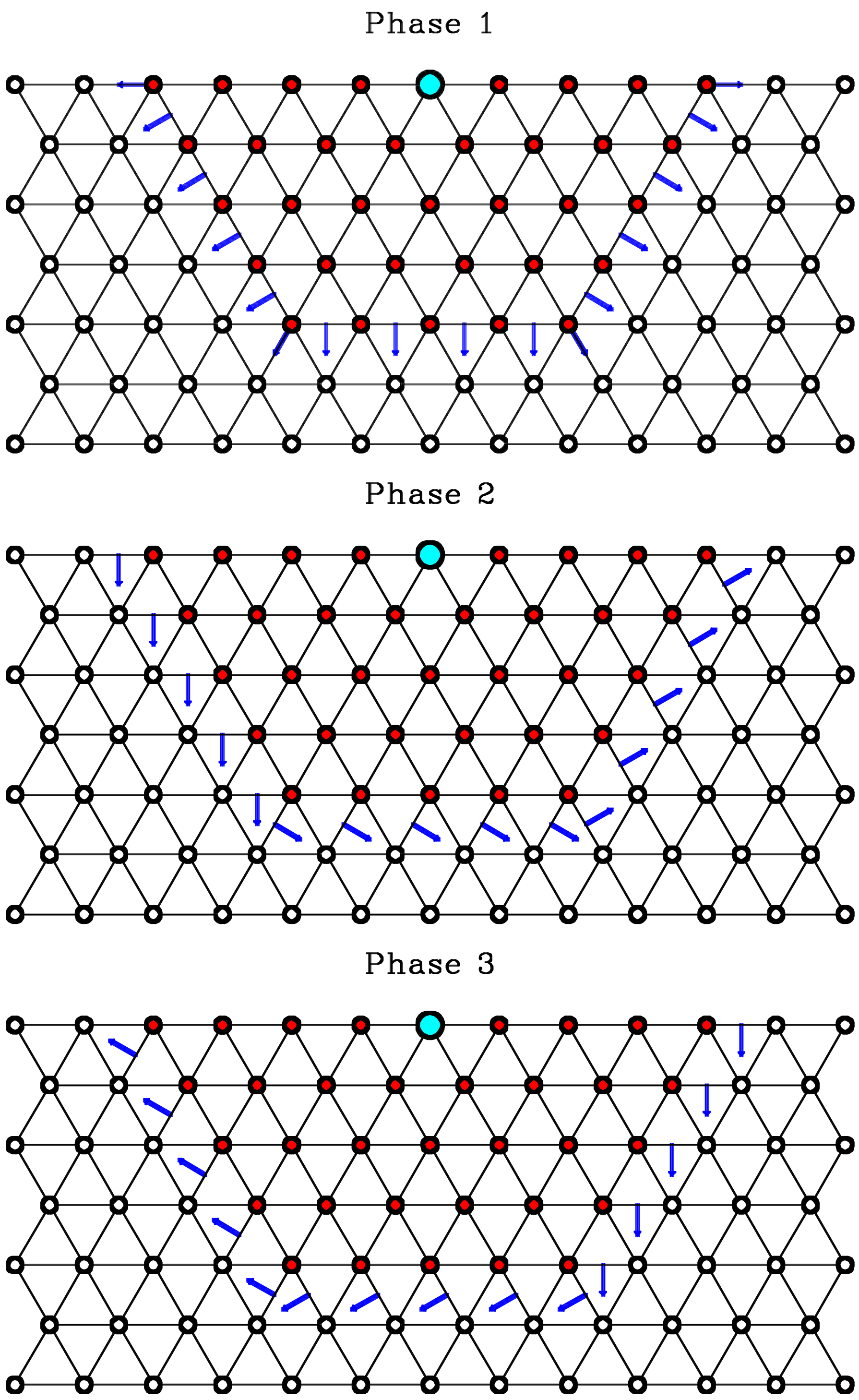

Figure 12: Three phases of the updating scheme in one step of wavefront propagation. Top: propagating out. Middle: propagating count-clockwise. Bottom: propagating clockwise. The big black dot shows the source position. The small black dots inside and on the half hexagonal ring of radius 4 shows the grid points at which the attributes of the wavefront are known. The arrows shows that the local wavefronts passing the boundaries attached by the ends of the arrows are propagated towards the grid points pointed by the arrows. $\boxed{\text{lin1-vpupdate}}$ [NR]

The velocity at the lower right corner of the model is 30. km/s. I use the local ray-tracing method to compute the attributes of wavefronts in this model. The grid size of the computation is 20 meters. Because the analytical solutions of the wavefronts attributes are known for such a medium, I plot the contours of the wavefront attributes calculated by the local ray-tracing method on the top of the contour plots of the corresponding analytical solutions. Figure 13 displays the contours of the traveltime and take-off angle fields. The contour intervals are 0.02 second for the traveltime field and 11.4 degrees for the take-off angle field. The contours of the traveltime and take-off angle fields show the trajectories of the wavefronts and rays, respectively. Because of the presence of the velocity gradient, the wavefronts are stretched in the direction of the velocity gradient and the rays are bended in the opposite direction of the velocity gradient. Figure 14 displays the contours of the fields of curvature radius of wavefront and geometrical spreading factor. The contour intervals are 0.4 km for the curvature radius field and 0.2 km for the geometrical spreading factor field. For a constant velocity model, these two fields are identical. The presence of large velocity gradient makes them quite different from each other. In both Figure 13 and Figure 14, the analytical solutions are plotted with white fat lines and the results of the local ray-tracing method are plotted with black thin lines. The near perfect match of two sets of contour lines indicates the high accuracy of the local-ray tracing method.

The second synthetic velocity model is a constant velocity field with a 50% negative Gaussian anomaly, and the third one with a 100% positive Gaussian anomaly, as shown in Figure 15. The size of anomalies is about 200 meters. I use the local ray-tracing method to compute the traveltime field of first arrivals in these models. The grid size used in the computations is 20 meters. In Figure 15, I compare the results of the traveltime calculations with the wave fields simulated by wave-equation modeling. Because a minimum phase wavelet is used in the wave-equation modeling, the contour lines of the traveltime fields closely follow the first breaks of the wavelets in the corresponding snapshots of the wave fields.

Multiple arrivals

I use the local ray-tracing method to compute the traveltime field in a two-layer velocity model. The velocities are 1.5 km/s in the top layer and 4.5 km/s in the bottom layer. After the critical angle, each point in the top layer has two arrivals: an arrival propagating directly from the source and an arrival refracted at the boundary of two layers. Therefore, the traveltime field is multi-valued in this region. I compute the traveltime field of multiple arrivals by applying the local ray-tracing method with three different selections: the first one selects the first arrivals, the second one selects the most energetic arrivals, and the third one selects upgoing arrivals. Figure 16 shows the contours of the three single-valued traveltime field. In the top layer, the first arrivals are the combinations of direct arrivals and diffracted arrivals, the most energetic arrivals are purely direct arrivals, and the upgoing arrivals have more

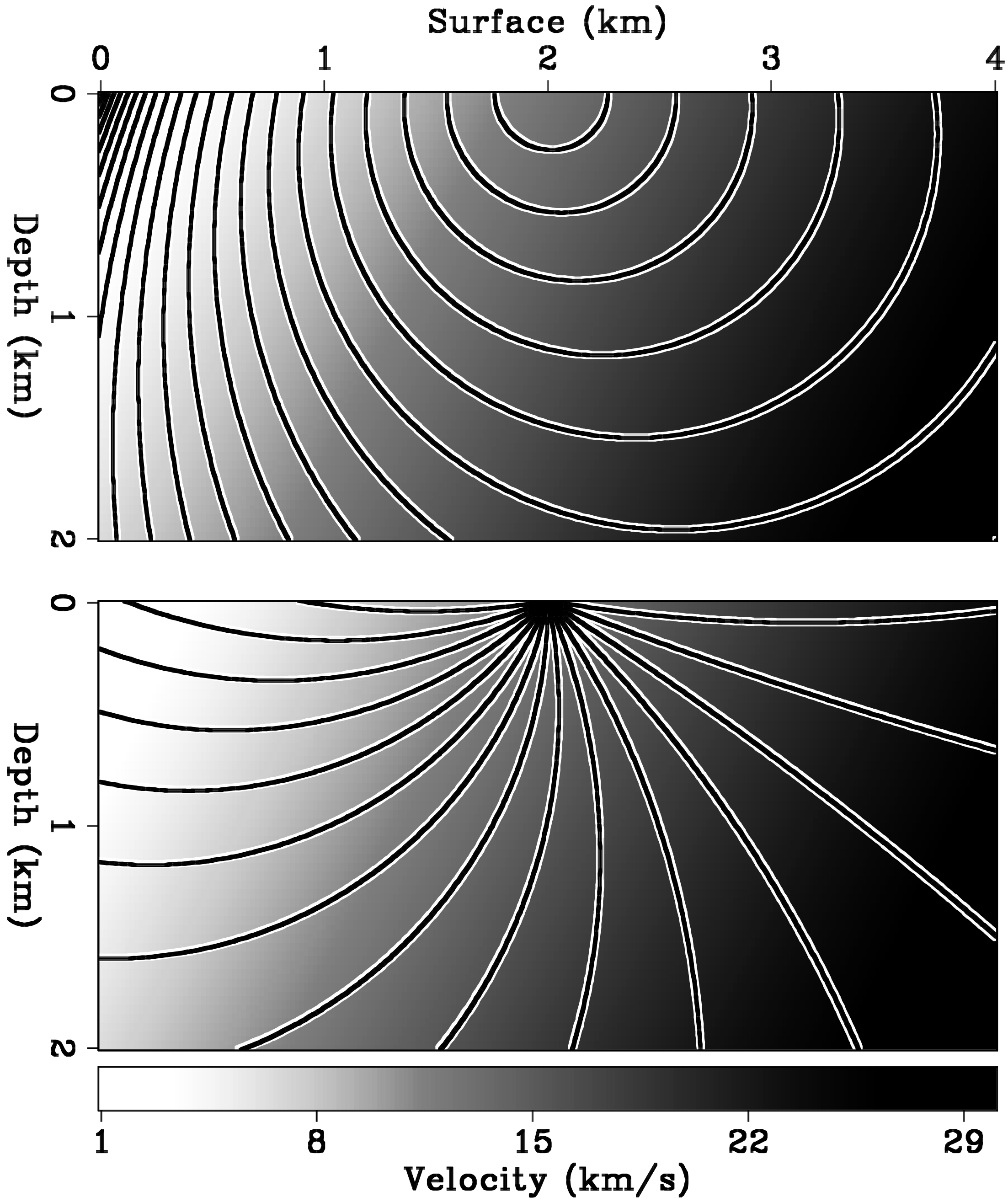

Figure 13: The wavefronts and rays in a linearly varying velocity model. The backgrounds of the two panels show the velocity field. The source is positioned at the top center of the model. The top panel shows the contour lines of the traveltime field with 0.02 second intervals. The bottom panel shows the contour lines of the take-off angle field with 11.4 degree intervals. The white lines shows the analytical solutions and the black lines show the results of the local ray-tracing method. lin1-ttmthgra [NR]

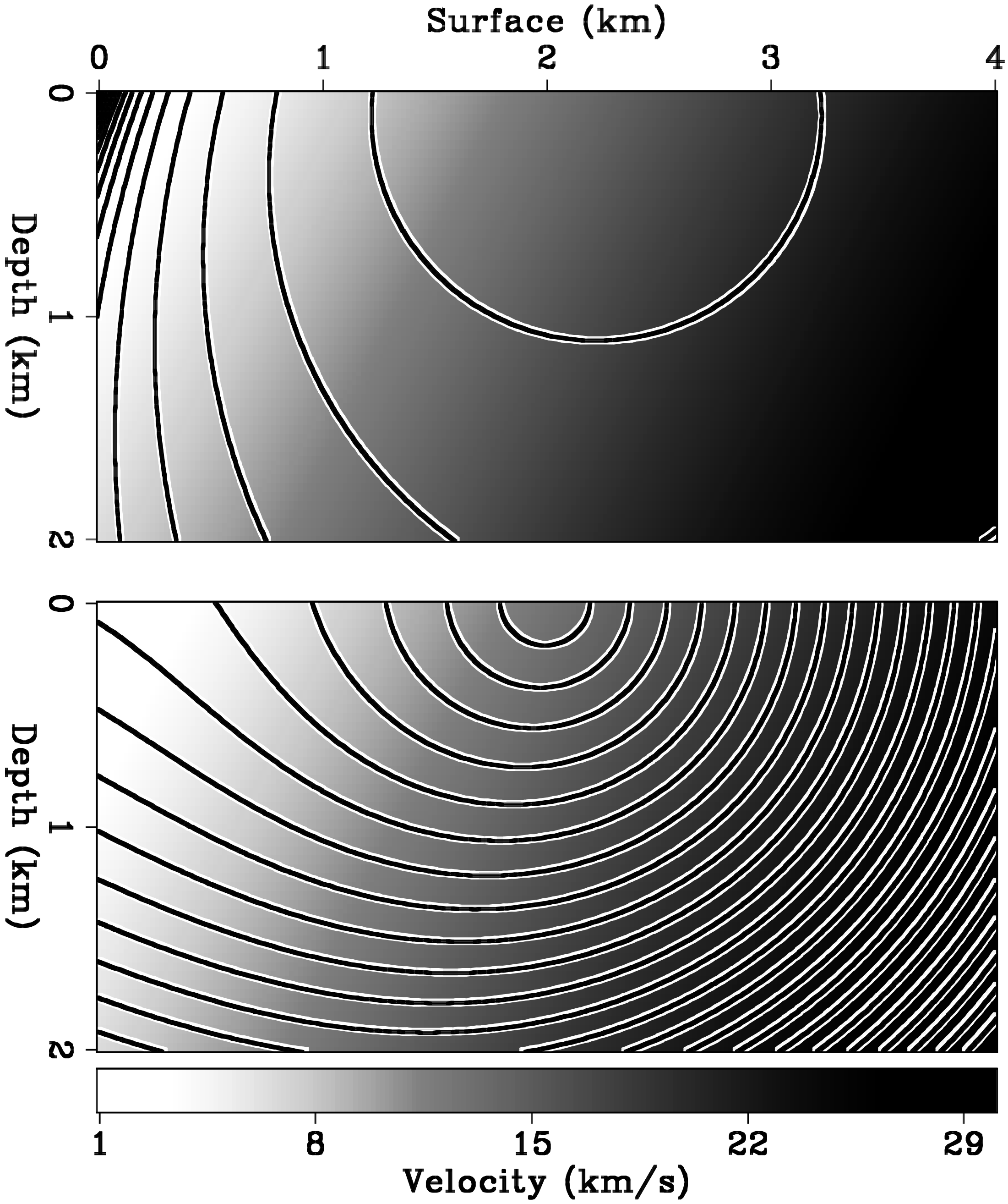

Figure 14: The curvature radii of wavefronts and geometrical spreading factors in a linearly varying velocity model. The backgrounds of the two panels show the velocity field. The source is positioned at the top center of the model. The top panel shows the contour lines of the curvature radius field with 0.4 km intervals. The bottom panel shows the contour lines of the geometrical spreading factor field with 0.2 km intervals. The white lines shows the analytical solutions and the black lines show the results of the local ray-tracing method. $\boxed{\text{lin1-rjjgra}}$ [NR]

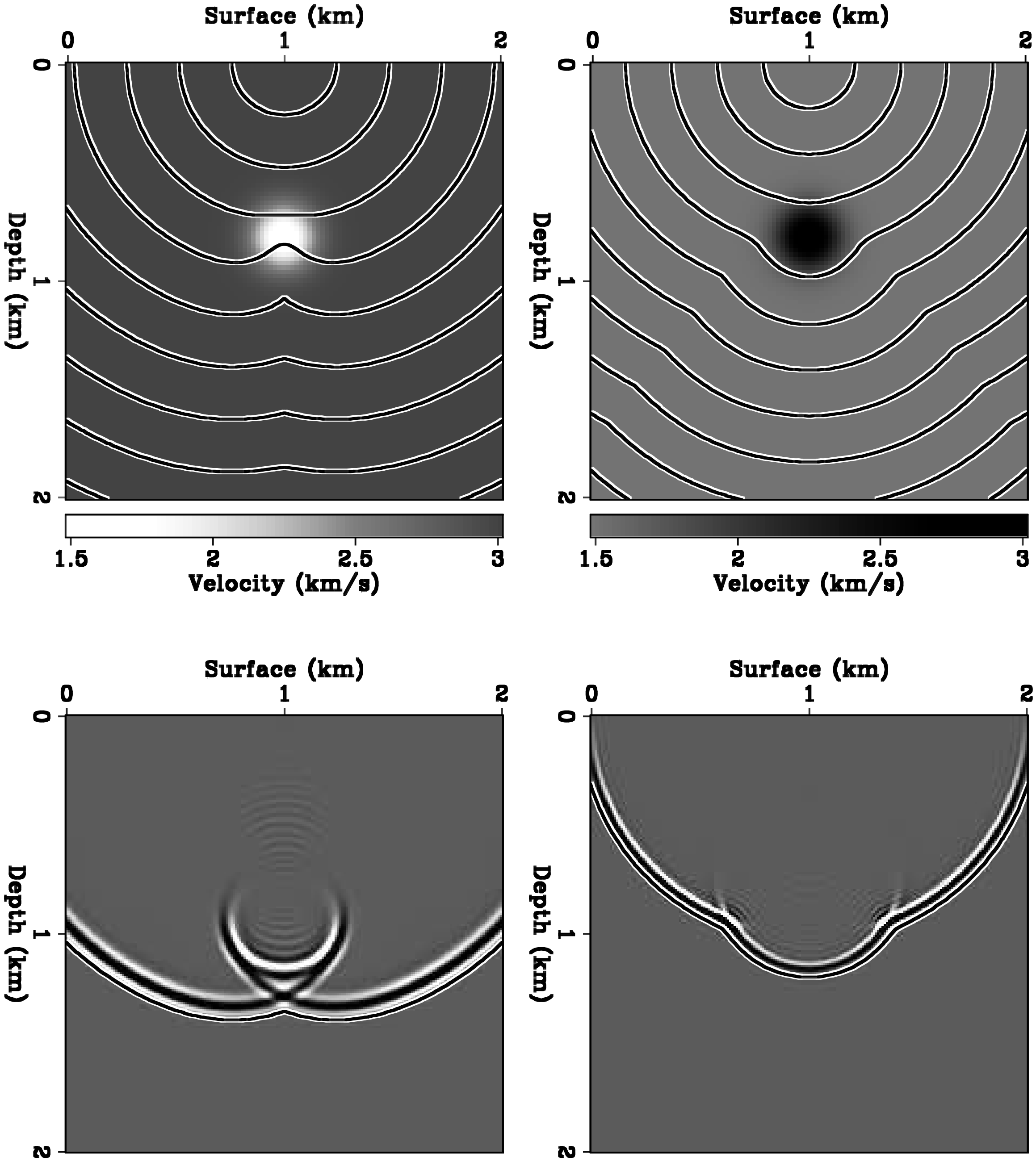

Figure 15: The wavefronts of first arrivals in velocity models with a negative Gaussian anomaly (left) and a positive anomaly (right). The backgrounds of the top panels show the velocity fields. Overlain are the contour lines of the traveltime fields. The contour interval is 0.08 second for the left panel and 0.14 for the right panel. The bottom panel compares the wave fields simulated by wave-equation modeling with the traveltime field calculated by the local ray-tracing method. The intensity plots show snapshots of the wave fields at 0.48 second (left) and 0.7 second (right); the overlain curves are the 0.48s-contour line (left) and 0.7s-contour line (right) of the traveltime fields. lin1-twpn [NR]

diffracted arrivals than the first arrivals. Three traveltime fields are identical in the bottom layer because each point there has only one arrival. The discontinuities of the contours are easy to identify. Figure 17 compares these results calculated by the local ray-tracing method with the wave field simulated by wave-equation modeling. Because a minimum phase wavelet is used in wave-equation modeling, the contour lines of the traveltime fields closely follow the first breaks of the wavelets in the corresponding snapshots of the wave fields.

As a final experiment, I compute the traveltime field in the Marmousi model shown in Figure 18. This synthetic velocity model has a complex geological structure with large velocity contrasts. Many regions in the model have multiple arrivals. The computation is conducted on a triangular grid with a grid size of 16 meters. Figure 18 shows the traveltime field of first arrivals in the Marmousi model. From the contour plot, we see that the circular wavefronts generated at the source point are severely distorted after propagate through the complex structure. The wavefronts propagate rapidly in the thin layers of high interval velocities. The comparison with the wave field computed by wave-equation modeling confirms accurate result of the local ray-tracing method. This experiment also shows that the local ray-tracing method is robust.

Figure 18 shows that the first arrivals at some regions are considerably weaker than later arrivals. Therefore, I compute another traveltime field by selecting most energetic arrivals. As shown in Figure19, the result on this model is not completely satisfactory. Although energetic arrivals at the shallow regions of the model are correctly computed, the method still picks up the weak arrivals diffracted at the boundaries of high-velocity thin layers. An explanation of this result is that the local ray-tracing method does not ensure global selections. The weak arrival propagating in the high-velocity thin layer may be strong at the early stage of the propagation.

CONCLUSIONS

I have presented a new method, named local ray-tracing method, for propagating wavefronts. Through the wavefront propagation process, the traveltimes and geometrical amplitudes of seismic waves are computed on an even grid, which is similar to a finite difference method for traveltime calculation. Because the method assumes a continuous velocity representation and propagates local circular wavefronts by following local rays, it gives more accurate traveltimes and amplitudes than a finite-difference method. The method can also compute the traveltimes of multiple arrivals. The traveltimes and amplitudes calculated by this method can be used in the Kirchhoff depth migration.

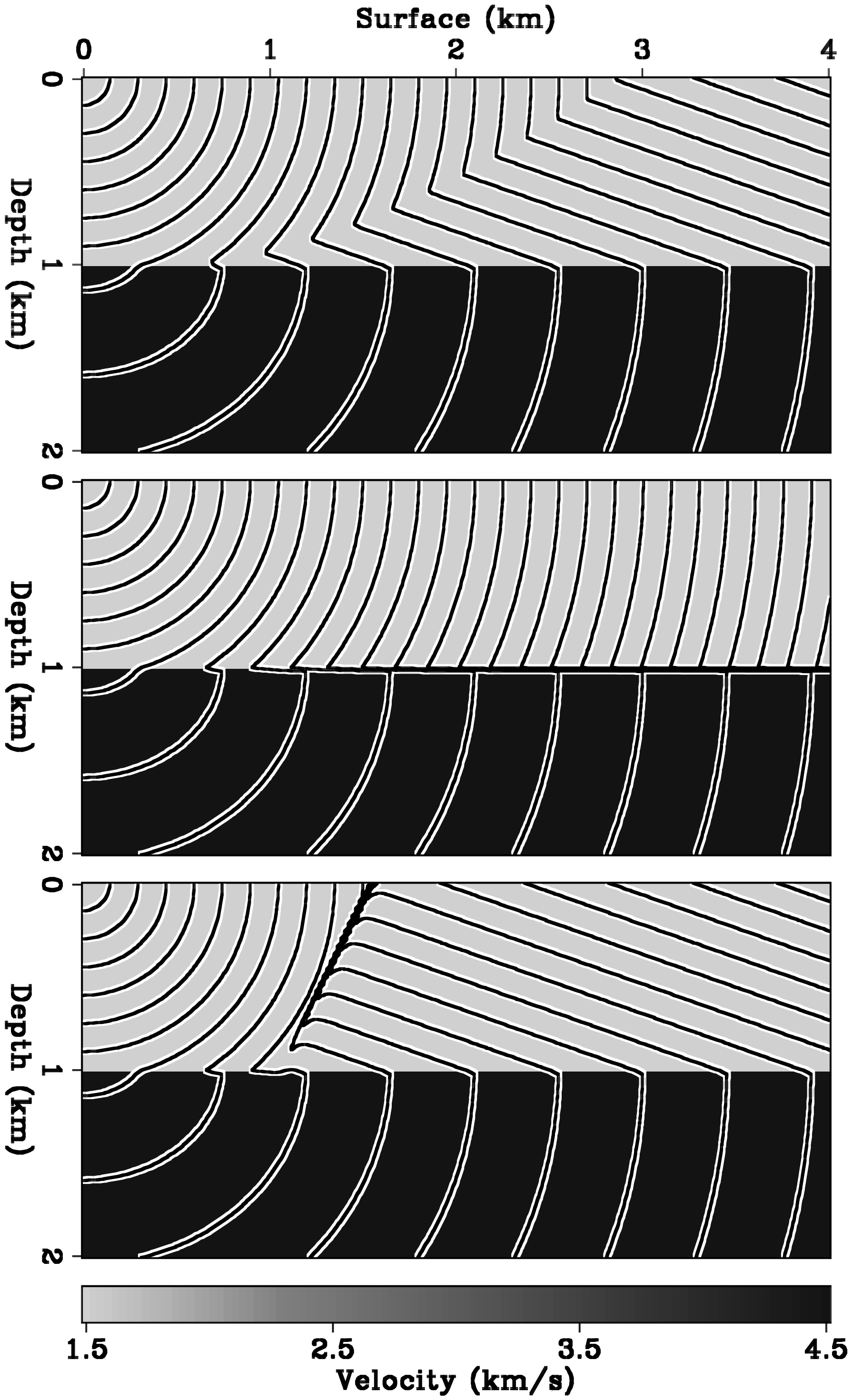

Figure 16: A point source positioned at the upper-left corner of the model generates a multi-valued traveltime field in a two-layer velocity model. This field is disassembled into three single-valued traveltime fields corresponding to first arrivals (top), most energetic arrivals (middle) and upgoing arrivals (bottom). The contour lines of three single-valued traveltime fields are plotted on the intensity backgrounds showing the velocity field. The contour interval is 0.1 second. lin1-ttmlay [NR]

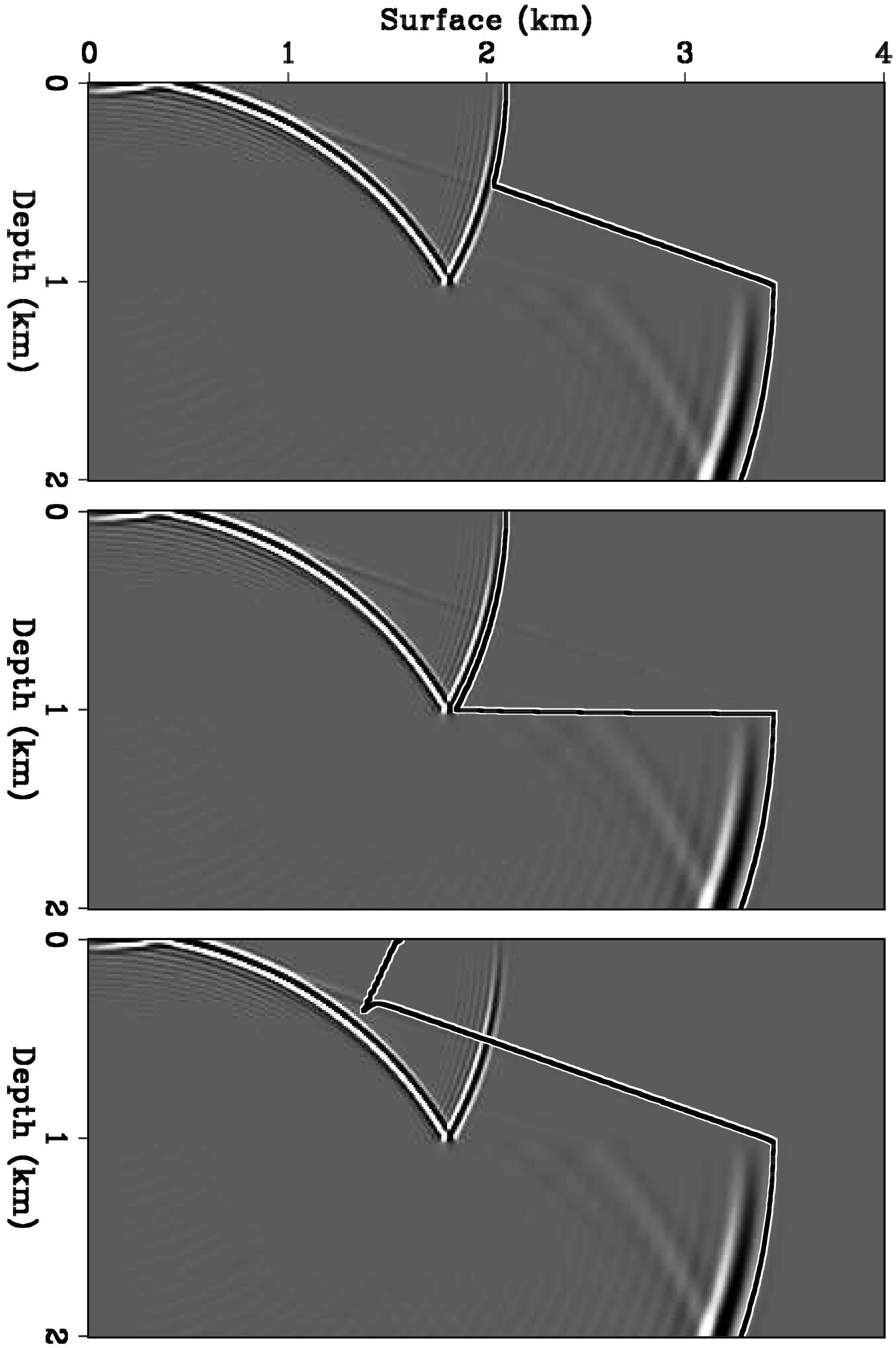

Figure 17: Comparison of the wave field simulated by wave-equation modeling with the traveltime fields calculated by the local ray-tracing method. The point source is positioned at the upper-left corner of the model. The intensity plots in three panels show a common snapshot of the wave field at 1.4 second; the overlain curves are the 1.4s-contour lines of three single-valued traveltime fields (see Figure 16). $\boxed{\text{lin1-wavelay}}$ [NR]

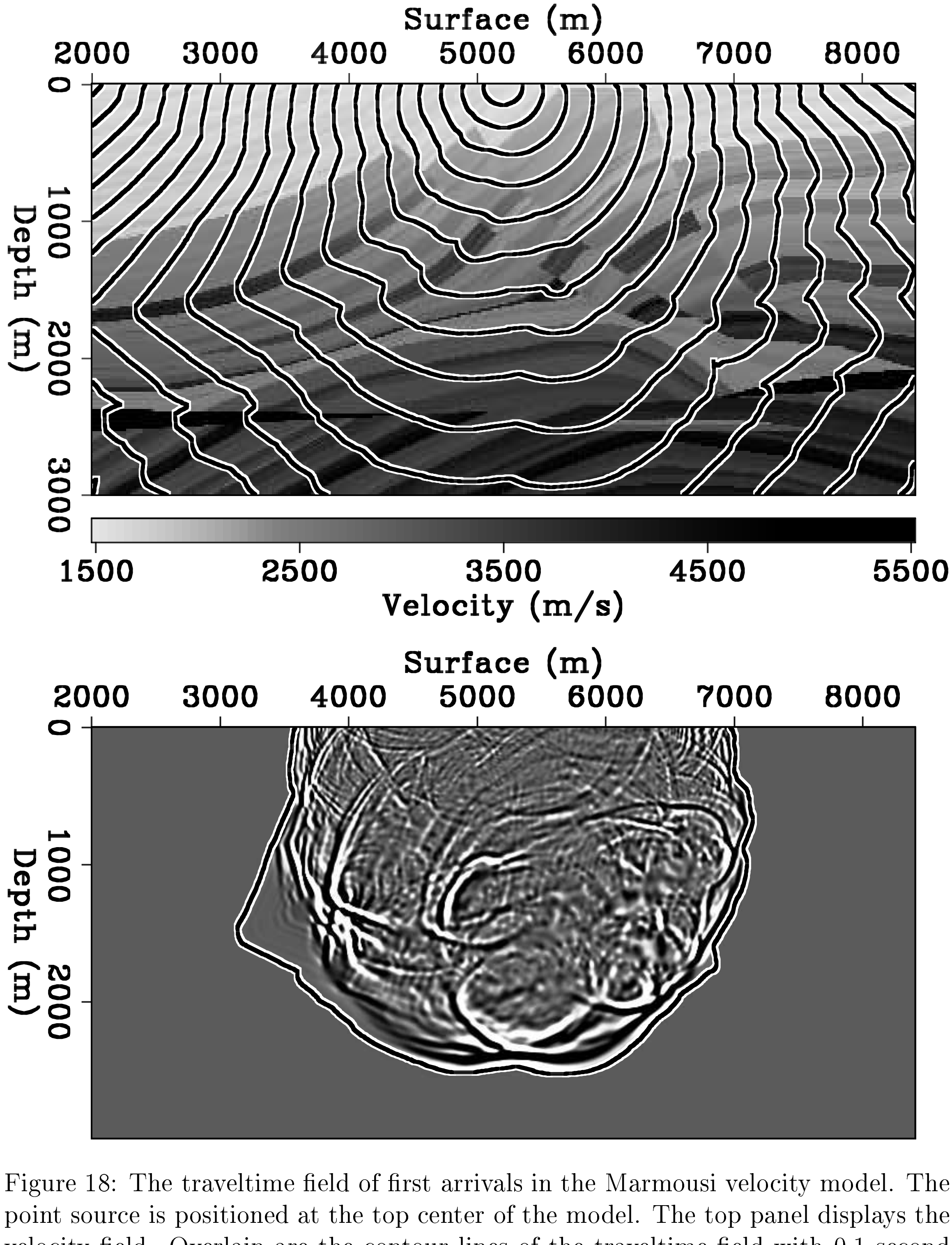

Figure 18: The traveltime field of first arrivals in the Marmousi velocity model. The point source is positioned at the top center of the model. The top panel displays the velocity field. Overlain are the contour lines of the traveltime field with 0.1 second intervals. The bottom panel compares the wave field computed by wave-equation modeling with the traveltime field calculated by the local ray-tracing method. The intensity plot shows a snapshot of the wave field at 1. second; the overlain curve is the 1.s-contour line of the traveltime field. lin1-twmar1 [NR]

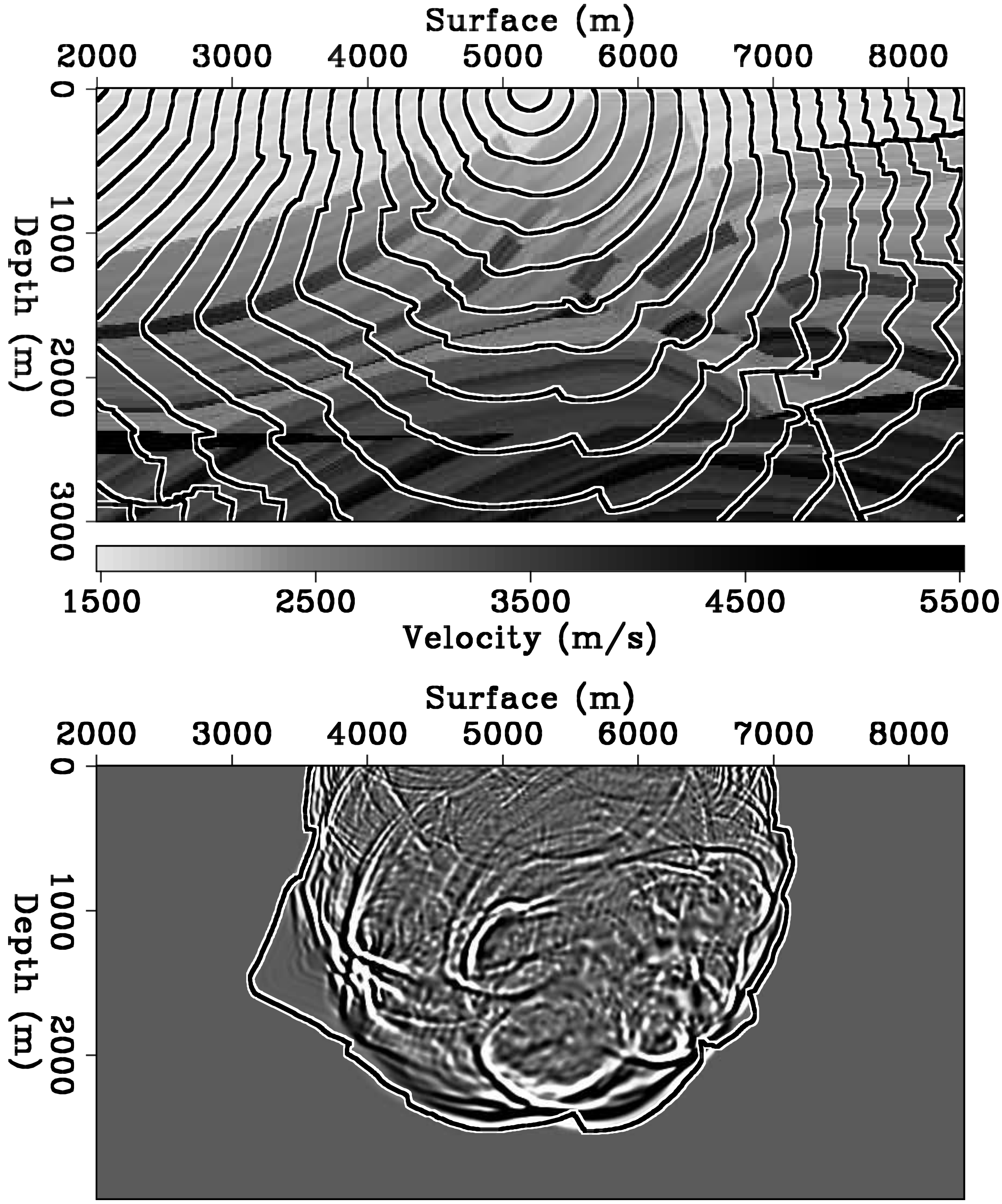

Figure 19: The traveltime field of most energetic arrivals in the Marmousi velocity model. The point source is positioned at the top center of the model. The top panel displays the velocity field. Overlain are the contour lines of the traveltime field with 0.1 second intervals. The bottom panel compares the wave field computed by wave-equation modeling with the traveltime field calculated by the local ray-tracing method. The intensity plot shows a snapshot of the wave field at 1. second; the overlain curve is the 1.s-contour line of the traveltime field. $\boxed{\text{lin1-twmar2}}$ [NR]

REFERENCES

Beydoun, W.B., and Keho, T.H., 1987, The paraxial ray method: Geophysics, **52**, 1639–1653.

Červený, V., 1981a, Ray tracing in a vicinity of a central ray: SEP–**28**, 39–48.

Červený, V., 1981b, Computation of geometrical spreading by dynamic ray tracing: SEP–**28**, 49–59.

Červený, V., 1981c, Dynamic Ray tracing across curved interfaces: SEP–**28**, 61–73.

Podvin, P., and Lecomte, I., 1991, Finite difference computation of traveltimes in very contrasted velocity models: a massively parallel approach and its associated tools: Geophys. J. Int., **105**, 271–284.

Van Trier, J., and Symes, W.W., 1991, Upwind finite-difference calculation of traveltimes: Geophysics, **56**, 812–821.

Vidale, J.E., 1988, Finite-difference calculation of travel times: Bull. Seism. Soc. Am., **78**, no. 6, 2062–2076.

Vidale, J.E., and Houston, H., 1990, Rapid calculation of seismic amplitudes: Geophysics, **55**, 1504–1507.

Zhang, L., 1991, Finite difference calculation of Green's functions: SEP–**72**, 153–169.